Aerosol and Air Quality Research, 18: 285–300, 2018

ISSN: 1680-8584 print / 2071-1409 online
doi: 10.4209/aaqr.2017.08.0263

Design and Performance Evaluation of a PN_1 Sensor for Real-Time Measurement of Indoor Aerosol Size Distribution

Junho Hyun[1], Jangseop Han[2], Sang-Gu Lee[1], Jungho Hwang[1,2*]

[1] *Graduate program of Clean Technology, Yonsei University, Seoul 03722, Korea*
[2] *Department of Mechanical Engineering, Yonsei University, Seoul 03722, Korea*

ABSTRACT

Airborne particulate matter is an important factor in the quality of an indoor environment. In this study, a miniaturized particle sensor was developed to detect submicron-sized aerosols based on number counting. This particle number (PN) sensor was designed and fabricated for real-time measurement of total aerosol number concentration and geometric mean diameter. The sensor (hereafter called as PN_1 sensor) comprised a particle-classification unit, a particle-charging unit, and a particle-detection unit. After integrating all the three units, the total number concentration and the geometric mean diameter of test aerosol particles were determined and the results were compared with those obtained using commercial instruments. First, the PN_1 sensor was compared with a condensation particle counter (CPC) in lab-test. For this, different groups of monodisperse sodium chloride particles between 20 and 700 nm in diameter were used. Then the PN_1 sensor was compared with a scanning mobility particle sizer (SMPS) and an aerodynamic particle sizer (APS). For this, the PN_1 sensor data were obtained by varying the combination of two corona voltage and test particles (sodium chloride and polystyrene latex) size distribution. In addition to lab-test, field test was carried out with indoor aerosols in different places. The number concentration and geometric mean diameter of indoor aerosols were measured by PN_1 sensor and compared with SMPS data. The number concentration was also compared with the results of CPC and Pegasor AQ Indoor (Pegasor, Finland) measurements.

Keywords: PN_1 sensor; Virtual impactor; Corona charger; Aerosol electrometer; Particle size distribution.

INTRODUCTION

Airborne particulate matter is an important factor in the quality of an indoor environment. In recent years, increasing public concern regarding air quality in residential and non-residential buildings has led to the development of efficient indoor aerosol-monitoring techniques. Several studies have reported that indoor aerosol particles are of submicron size because these particles are generated, for example, by cooking, human activities, or cleaning (Abt *et al.*, 2000; Long *et al.*, 2000; Morawska *et al.*, 2003). Exposure to submicron-sized particles has an impact on human health when we inhale and the particles enter the body. Particles that are a few microns in diameter are blocked by hair in the nostrils; however, submicron-sized particles can reach the lungs and deposit in the alveoli (Mitsakou *et al.*, 2007).

Real-time aerosol number concentration can be measured using two existing methods: optical and electrical. The optical method typically uses light-scattering technology. However, for particles smaller than approximately half the wavelength of the light used for the measurement, the scattering intensity scales with particle diameter d as d^6, implying that the light-scattering intensity drops very rapidly for particles < 0.3 μm (Fierz *et al.*, 2011). If the measured aerosol and the properties of the sensor are known, the measured electrical signal can be converted, for instance, into a number concentration (Rostedt *et al.*, 2009) and a particle size (Zhang *et al.*, 2016). Therefore, many studies have focused on electrical methods for measuring these submicron particles.

Although commercially available particle-detection systems based on electrical methods have been successful to some extent, they are large and expensive, e.g., the dimension of an electrical low-pressure impactor (ELPI, DEKATI, Finland) is 400 × 230 × 570 mm^3 (width × depth × height). Therefore, there is an immediate need for compact and easy-to-deploy miniature particle-detection instruments. Fierz *et al.* (2008, 2011) introduced a diffusion-size classifier (DiSC) for real-time measurements of particle concentration and particle diameter over a size range from 20 to 240 nm. The DiSC is a simple instrument based on unipolar charging of the aerosol, followed by detection in

*Corresponding author.
Tel.: 82-2-2123-2821; Fax: 82-2-312-2821
E-mail address: hwangjh@yonsei.ac.kr

two electrometer stages. It was commercialized by Matter Aerosol as DiSCmini (size range = 10–700 nm). Marra *et al.* (2010, 2011) reported that the Aerasense NanoTracer, which was commercialized by Philips (NanoTracer), enabled intelligence gathering with respect to airborne particles; in particular, in the 10–300 nm size range. The functionality of NanoTracer relies on electrical charging of airborne particles and subsequent measurements of the total particle-charge concentration under various conditions.

Both the DiSCmini and NanoTracer are compact and portable. Asbach *et al.* (2012) compared five different portable nanoparticle monitors, including the NanoTracer, and found that the results provided by the NanoTracer were consistent with condensation particle counter (CPC) for sodium chloride (NaCl) particles having 37.8 nm of geometric mean diameter. Mills *et al.* (2013) evaluated the DiSCmini for measuring the number concentration and geometric mean diameter of test NaCl particles by comparing with CPC and scanning mobility particle sizer (SMPS). For test NaCl particles, three monodisperse particle groups of 30, 100, and 300 nm in diameter, respectively, were used. They reported that the accuracy of the DiSCmini was reasonable for the two groups of 30 and 100 nm particles, but that caution was needed for the group of 300 nm particles.

For the present study, we designed and fabricated a miniaturized particle sensor (10 cm height × 20 cm width × 15 cm length) for real-time measurement of total indoor aerosol number concentration and geometric mean diameter. The sensor detected particles, whose size range was 20 to 1000 nm, based on number counting (hereafter called as PN_1 sensor). Sodium chloride (NaCl) particles of 20–700 nm and polystyrene latex (PSL) particles of 500–1000 nm were used in the laboratory test. Field test was carried out with ambient aerosols in different places. Assuming a log-normal distribution with given geometric standard deviation, the total number concentration and the geometric mean diameter of particles were estimated. For this, an equation was theoretically developed and two different electrical currents corresponding to two different charger voltages, respectively, were applied to the equation. Finally, the results were compared with those obtained from a commercial SMPS and aerodynamic particle sizer (APS).

METHODS

PN_1 Sensor

As shown in Fig. 1, the sensor is composed of a particle-classification unit, a particle-charging unit, and a particle-detection unit. The total weight of the sensor (including a pump) is about 7 kg. A virtual impactor with cut-size of 1 μm is used as the particle-classification unit. The general mechanism of a virtual impactor involves separating aerosol particles into a straight low-velocity flow (minor flow) and a perpendicular high-velocity flow (major flow). High-inertia particles are unable to navigate the turn into the major flow, so they are concentrated into the minor flow. The bottom of the impactor is made of Bakelite and the top of the impactor is made of polyvinyl chloride to prevent flow leakage. The width, length, and height of the impactor are 45, 45, and 10 mm, respectively.

A wire-to-rod-type corona charger serves as the particle-charging unit. The charger is designed to generate highly charged submicron aerosol particles. A high positive DC voltage applied to the discharge wire produces positive gaseous ions. The particles entrained from the particle classification unit by carrier air should be positively charged due to their collision with migrated positive ions. The main body of the charger is ceramic, which stabilizes the corona discharge. The width, length, and height of the charger are 30, 30, and 29 mm, respectively. The discharge wire has a radius of 20 μm and is made of tungsten, whereas each ground rod has a radius of 1 mm and is made of stainless steel. The discharge wire is separated from the ground rod by 3 mm.

Charged particles enter the particle-detection unit and the electrical current they carry is measured by using a lab-

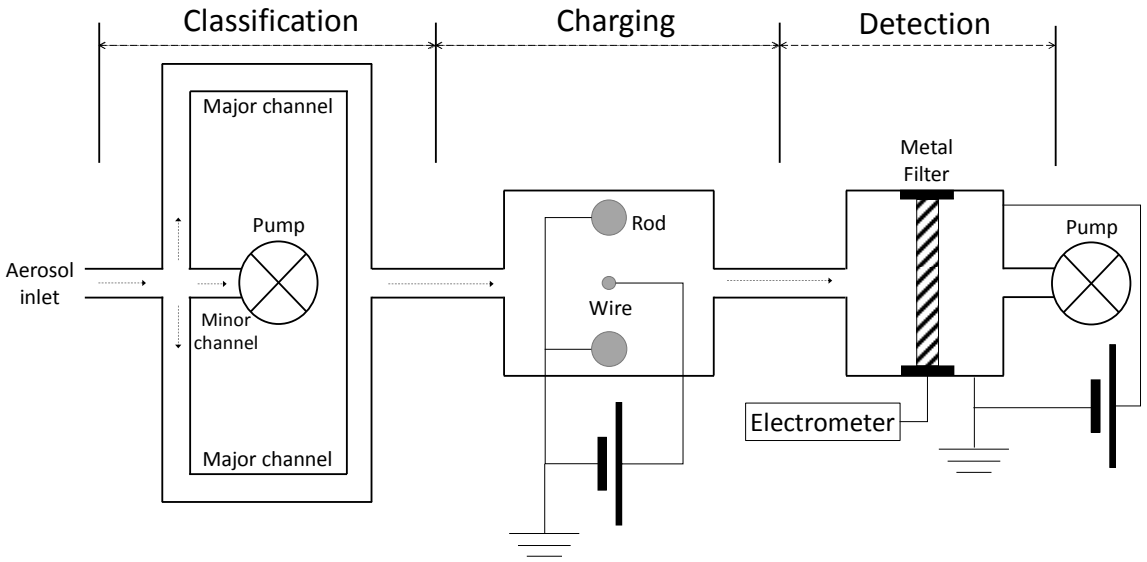

Fig. 1. Schematic diagram of PN_1 sensor.

made aerosol electrometer. Assuming that the particles have a log-normal size distribution with given geometric standard deviation, the total number concentration and the geometric mean diameter are estimated by using a theoretically developed equation. In the equation two electrical currents corresponding to two different charger voltages, respectively, are used. Our lab-made aerosol electrometer is composed of a Faraday cage and an electrometer. Particles in the sample flow are collected in a metal high-efficiency particulate air (HEPA) filter housed in an epoxy glass enclosure, with the whole constituting a Faraday cage. The metal HEPA filter is made by ASFLOW Corporation in Korea and is based on sintered porous-metal media fabricated from nickel metal powder. The width, length, and height of the Faraday cage are all 30 mm.

Design and Performance Evaluation of Virtual Impactor

The geometric design parameters of the virtual impactor are shown in Supplemental information. In general, the nozzle width (W), the jet-to-plate distance (S), and the nozzle thickness (t) are directly related to the degree of particle separation achieved by the impactor. The design of the impactor considers the following dimensionless parameters: Stokes number (Stk), jet Reynolds number (Re), and the ratio S/W. The Stokes number is the ratio of the stopping distance of a particle to the half width. The cutoff diameter (d_{50}) is defined as the aerodynamic diameter that gives 50% collection efficiency. The value of Stk often used to characterize an inertial impactor is Stk_{50}.

In this study, the nozzle width (W) and thickness (t) are both 1 mm to achieve a 1 μm cutoff diameter. Assuming Stk_{50} = 0.23 for a rectangular nozzle (Sioutas *et al.*, 1994), the inlet flow rate (Q_{inlet}) is calculated to be 4.0 L min^{-1}. The jet-to-plate distance (S) is then determined from the injection-nozzle width (W) because the minimum ratio S/W should remain within the range 1.2–1.8 (Loo and Cork, 1988). In this study, we use S/W = 1.5.

To determine the major and minor flow rates for a given Q_{inlet} (4.0 L min^{-1}), the computational fluid dynamic (CFD) software FLUENT was used to simulate fluid flow and particle motion. Starting with the ratio Q_{minor}/Q_{inlet} = 0.1, the flow field distribution was calculated by solving the steady-state mass- and momentum-conservation equations, with the boundary conditions given in Supplemental information. After solving the flow field, particle trajectories were calculated by using a Lagrangian approach (Discrete Phase Model) included in FLUENT. Sixty particles of the same size were assumed to enter the impactor starting at different inlet locations. Therefore, all 60 particles followed different trajectories; some of them flowed into the major channel, some flowed straight into the minor channel, and others were deposited on the interior of the walls. Particle sizes ranging from 0.5 to 1.5 μm were used. The separation efficiency (SE_c) and wall loss (WL_c) for each particle size were calculated as follows:

$$SE_c(d_p) = \frac{\tilde{N}_{\text{minor}} \sum (u_i A_i)_{\text{minor}}}{\tilde{N}_{major} \sum (u_i A_i)_{major} + \tilde{N}_{\text{minor}} \sum (u_i A_i)_{\text{minor}}}, \quad (1)$$

$$WL_c(d_p) = \frac{\tilde{N}_{major} \sum (u_i A_i)_{major} + \tilde{N}_{\text{minor}} \sum (u_i A_i)_{\text{minor}}}{\tilde{N}_{\text{inlet}} \sum (u_i A_i)_{\text{inlet}}}, \quad (2)$$

where $\tilde{N}_{\text{inlet}}$, $\tilde{N}_{major}$, and $\tilde{N}_{\text{minor}}$ are the numbers of particles at the inlet, major, and minor channels, respectively, and u and A are the flow velocity and the cross-sectional area, respectively. The subscript i is the number of the calculation cell in each channel. So, the calculation of SE_c for various particle sizes was done with Q_{minor}/Q_{inlet} = 0.1. This procedure was repeated with different values of Q_{minor}/Q_{inlet} until the calculated cutoff diameter approached 1 μm.

After determining the geometric design parameters and flow rates of the virtual impactor, we fabricated the impactor and evaluated its performance with the experimental setup shown in Fig. 2(a). Compressed air was used as a carrier gas after using a clean-air supply to remove oil droplets, moisture, and contamination particles. This supply consisted of an oil trap, a diffusion dryer, and a HEPA filter. Polystyrene latex (PSL) particles (density of 1.054 g cm^{-3}) of 0.5, 0.65, 0.75, 0.82, 0.93, 1, 1.2, 1.3, and 1.5 μm in diameter were generated from an atomizer (9302, TSI, MN, USA). The airflow rate to the atomizer was maintained at 3.0 L min^{-1}. The PSL particles entered the virtual impactor after first passing through a diffusion dryer and then a soft X-ray type aerosol neutralizer (4530, HCT, Korea). To obtain the separation efficiency and wall loss, we measured the number concentration of particles at the inlet (N_{inlet}) and the concentrations at the two exits (N_{major} and N_{minor}) by using an APS (3321, TSI, MN, USA). The APS measures particles from 0.5 to 20 μm in aerodynamic diameter by using a double-crest optical system, and the aerosol sample flow rate and the sheath air flow rate are 1.0 and 4.0 L min^{-1}, respectively. The experimentally determined separation efficiency SE_m and wall loss WL_m were obtained by using

$$SE_m(d_p) = \frac{N_{\text{minor}}(d_p)\, Q_{\text{minor}}}{N_{major}(d_p)\, Q_{major} + N_{\text{minor}}(d_p)\, Q_{\text{min or}}}, \quad (3)$$

$$WL_m(d_p) = 1 - \frac{N_{major}(d_p) Q_{major} + N_{\text{minor}}(d_p) Q_{\text{minor}}}{N_{inlet}(d_p) Q_{inlet}}. \quad (4)$$

where Q_{inlet}, Q_{major}, Q_{minor} represent the flow rates at the inlet, major channel, and minor channel, respectively.

Design and Performance Evaluation of Charger

To obtain higher particle charge, higher ion concentration is required. The ion concentration (N_{ion}) is estimated by using

$$N_{ion} = \frac{I_C}{eZ_i EA} \quad (5)$$

where I_c is the corona current, Z_i is the mobility of positive air ions (1.4 cm^2 V^{-1} s^{-1}), E is the mean value of the electric field intensity, e is the elementary unit of charge (1.6 × 10^{-19} C), and A is the inner surface area of the

ground electrode. The corona current can be expressed by using the general empirical formula for the current-voltage relation reported by Meng *et al.* (2008),

$$I_{corona} = C(V - V_0)^a \tag{6}$$

where C and a are the constants determined by the electrode geometry, V is the voltage applied on the discharge wire, and V_0 is the corona starting voltage. The exponent a is in the range 1.5–2.0. When the applied voltage exceeds the breakdown voltage, the electric field intensity exceeds the dielectric field strength of air (3 MV m^{-1}) and a spark is triggered. To produce a corona discharge, the electric field strength must exceed the corona starting electric field. When two distant, parallel, and unequal cylindrical conductors are used as electrodes, the corona starting voltage V_0 is calculated by using

$$\mathrm{V}_0 = 2E_0 r_w \ln\left[\frac{d}{\sqrt{r_w r_r}}\right], \text{ for } d \gg r_r, \tag{7}$$

where r_w and r_r are the radii of the discharge wire and ground rod, respectively, and d is the distance between the wire and the rod (Kaiser, 2006). The corona starting electric field E_0 is defined as

$$E_0 = f(3.1\times10^6)\left[\delta + 0.0308\left(\frac{\delta}{r_w}\right)^{0.5}\right] \tag{8}$$

where f is a factor that accounts for wire roughness (f = 1 in this study) and δ is the correction coefficient for temperature and pressure (δ = 1 in this study).

To test the electrical characteristics of our charger, corona currents (I_{corona}) according to various applied voltages (V) were measured by using an oscilloscope (WaveRunner 6050A, Lecroy, NY, USA). After checking the current-voltage characteristics, we evaluated the particle loss and charging characteristics of the charger by using the setup shown in Fig. 2(b). PSL particles having diameter of 500, 600, 700, 820, 1000 nm were generated from an atomizer. Sodium chloride (NaCl) particles of 20–700 nm were also used; they were generated from an electrically heated tube furnace (GTF12/25/364, Lenton Furnaces, UK) with clean air exhausted from the clean air supply system. The heating length and inner diameter of the ceramic tube were 364 and 25.4 mm, respectively. The airflow rate supplied to the ceramic tube was maintained at 2.0 L min^{-1}. Once the NaCl particles were generated, the desired NaCl particle concentration was controlled by using a dilutor. To supply monodisperse NaCl particles for each particle size to the charger, the particles were classified by a differential mobility analyzer (DMA, 3081, TSI, MN, USA) after passing through a charge neutralizer. The particle flow of 0.3 L min^{-1} exhausted from the DMA was controlled by a laminar flow meter and was mixed with 2.9 L min^{-1} of clean air by another diluter. Next, the particles mixed with clean air were exposed to another neutralizer. The charge-redistributed particles passed through an electrostatic precipitator (ESP) (Ji *et al.*, 2004) to remove the charged particles. The ESP consisted of a cylindrical brass housing containing an expander inlet, a central electrode, and a converging nozzle outlet. The ESP was designed to remove both positively and negatively charged particles by applying a voltage of 200 V to the central electrode and grounding the housing. The free ions leaving the charger were removed by using an ion trap. The voltage applied in the ion trap was 20 V.

The particle wall loss (WL_{charger}) was defined as the ratio of the outlet concentration of particles to the inlet concentration of particles through the charger, as follows;

$$WL_{charger}(d_p) = \frac{N_1(d_p) - N_2(d_p)}{N_1(d_p)}, \tag{9}$$

where $N_1(d_p)$ is the number concentration of aerosol particles entering the charger (# cm^{-3}) and $N_2(d_p)$ is the concentration of aerosol particles exiting the charger when a high voltage is applied to the charger. The number concentration is measured by CPC (3776, TSI, MN, USA).

The average particle charge per particle size (n_m) was estimated by using

$$n_m(d_p) = \frac{I(d_p)}{N_2(d_p)eQ}, \tag{10}$$

where Q is the flow rate and $I(d_p)$ is the current of aerosols exiting the charger when a high voltage is applied to the charger. The current was measured by an aerosol electrometer (3068B, TSI, MN, USA).

Design and Performance Evaluation of Lab-Made Aerosol Electrometer

A filtration test of the metal HEPA filter in the Faraday cage was done by using the experimental setup shown in Fig. 2(c). To insert the monodisperse NaCl particles, the particles were classified by DMA after they passed through a charge neutralizer. The particle flow of 0.3 L min^{-1} exhausted from the DMA was controlled by a laminar flow meter and was mixed with 2.9 L min^{-1} of clean air by a diluter. The particle number concentrations were measured by CPC upstream and downstream from the Faraday cage. The particle removal efficiency of the HEPA filter, $\eta_{filter}(d_p)$, was defined as

$$\eta_{filter}(d_p) = 1 - \frac{N_{down}(d_p)}{N_{up}(d_p)} \tag{11}$$

where $N_{down}(d_p)$ is the number concentration of downstream particles with size d_p and $N_{up}(d_p)$ is the number concentration of upstream particles with size d_p. The results of filtration tests are given in Supplemental information.

Fig. 2(d) shows a schematic drawing of the experimental setup for measuring the electrical current with our lab-made aerosol electrometer, which consists of an electrometer and the Faraday cage. The circuit diagram and results of

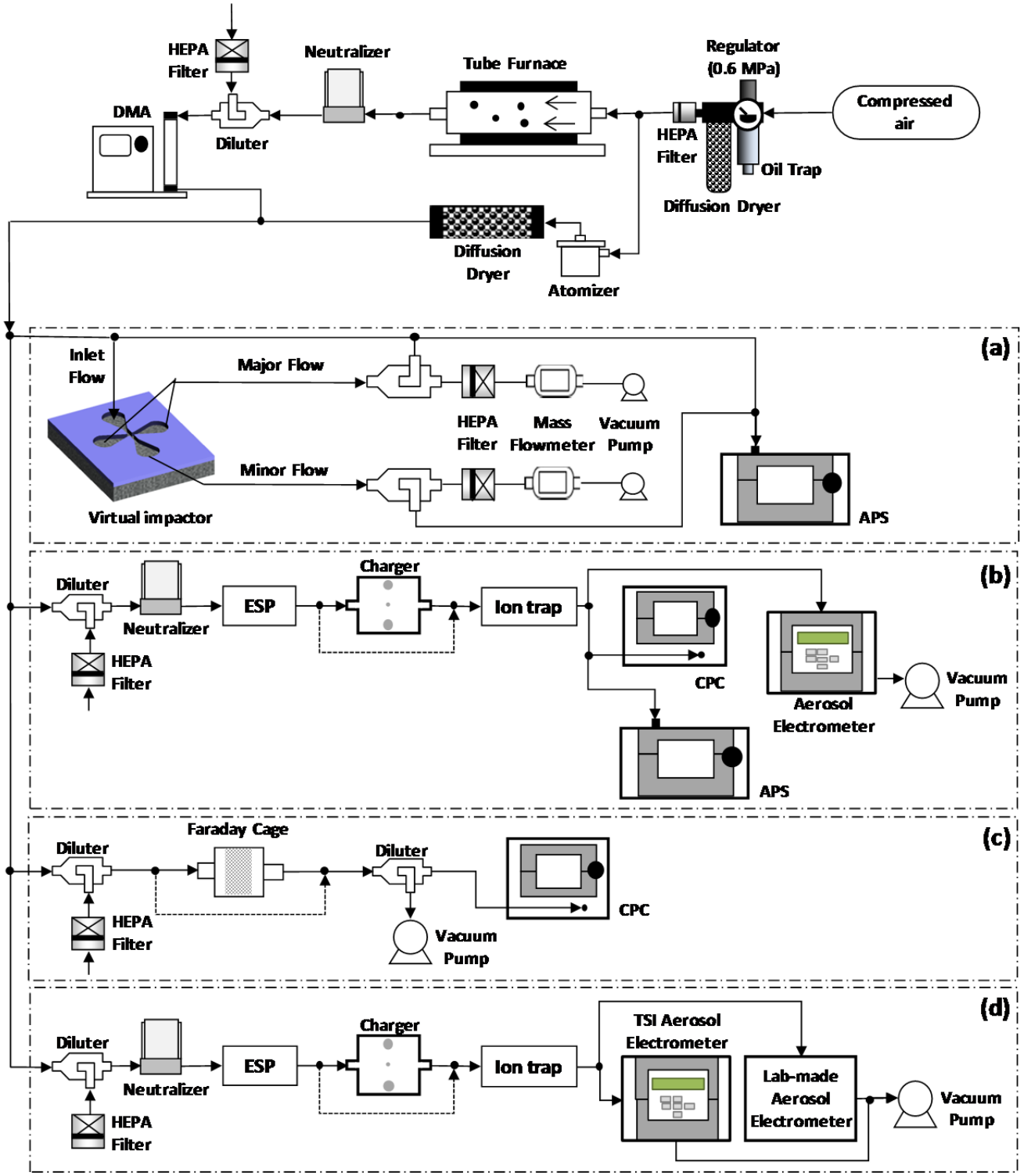

Fig. 2. Experimental setups for (a) Separation efficiency test of impactor, (b) Charging characteristics test of charger, (c) Filtration efficiency test of Faraday cage, and (d) Comparison test of lab-made aerosol electrometer with TSI aerosol electrometer.

the performance test of the electrometer are shown in Supplemental information. The lab-made aerosol electrometer was compared with the TSI aerosol electrometer for given particle size (from 20 to 1000 nm) and number concentration (from 40 # cm^{-3} to 30,000 # cm^{-3}). To insert monodisperse NaCl particles for each particle size, the particles were classified by DMA after passing through a charge neutralizer. The particle flow of 0.3 L min^{-1} exhausted from the DMA was controlled by a laminar flow meter and was mixed with 2.9 L min^{-1} of clean air by using a diluter. After the

free ions leaving the charger were removed with an ion trap, the current carried by the particles was measured by each aerosol electrometer. SPSS (SPSS Inc., version 21, IBM Corporation) was used to do the statistical analysis. The correlation analysis was calculated by using Pearson's product moment and significances of differences between aerosol electrometers were calculated by using a Student's t-test at a significance level of 5%.

Estimation of Number Concentration and Size Distribution with PN_1 Sensor

Fig. 3 shows schematic diagrams for number concentration and geometric mean diameter measurements. NaCl particles and PSL particles were generated from the tube furnace and the Collison-type atomizer, respectively, and passed through a soft X-ray type aerosol neutralizer. The number concentration was measured by PN_1 sensor and the results were compared with CPC data (see Fig. 3(a)). Then the geometric mean diameter was measured by PN_1 sensor and the results were compared with SMPS (3936L76, TSI, MN, USA) data for NaCl particles and APS data for PSL particles. The following equations were used to determine the number concentration and geometric mean diameter with PN_1 sensor.

The electrical current carried by charged particles is expressed as (Park *et al.*, 2010)

$$I = e \cdot Q \int p \cdot n_m(d_p) \cdot n(d_p) dd_p \tag{12}$$

The product $p \cdot n_m$ is a function of the particle diameter (d_p), expressed as follows;

$$p \cdot n_m(d_p) \approx a \times d_p^{\beta} \tag{13}$$

where the unit of d_p is nanometers, and α and β are constants that depend on the voltage applied to the charger. With the assumption that the particle sizes follow a unimodal log-normal distribution, the particle size distribution $n(d_p)$ becomes

$$\frac{n(d_p)}{N_{total}} = \frac{1}{d_p \sqrt{2\pi} \ln \sigma_g} \exp\left(\frac{-(\ln d_p - \ln d_{pg})^2}{2 \ln^2 \sigma_g} \right), \tag{14}$$

where N_{total} is the total number concentration and d_{pg} is the geometric mean diameter. It is also assumed that the

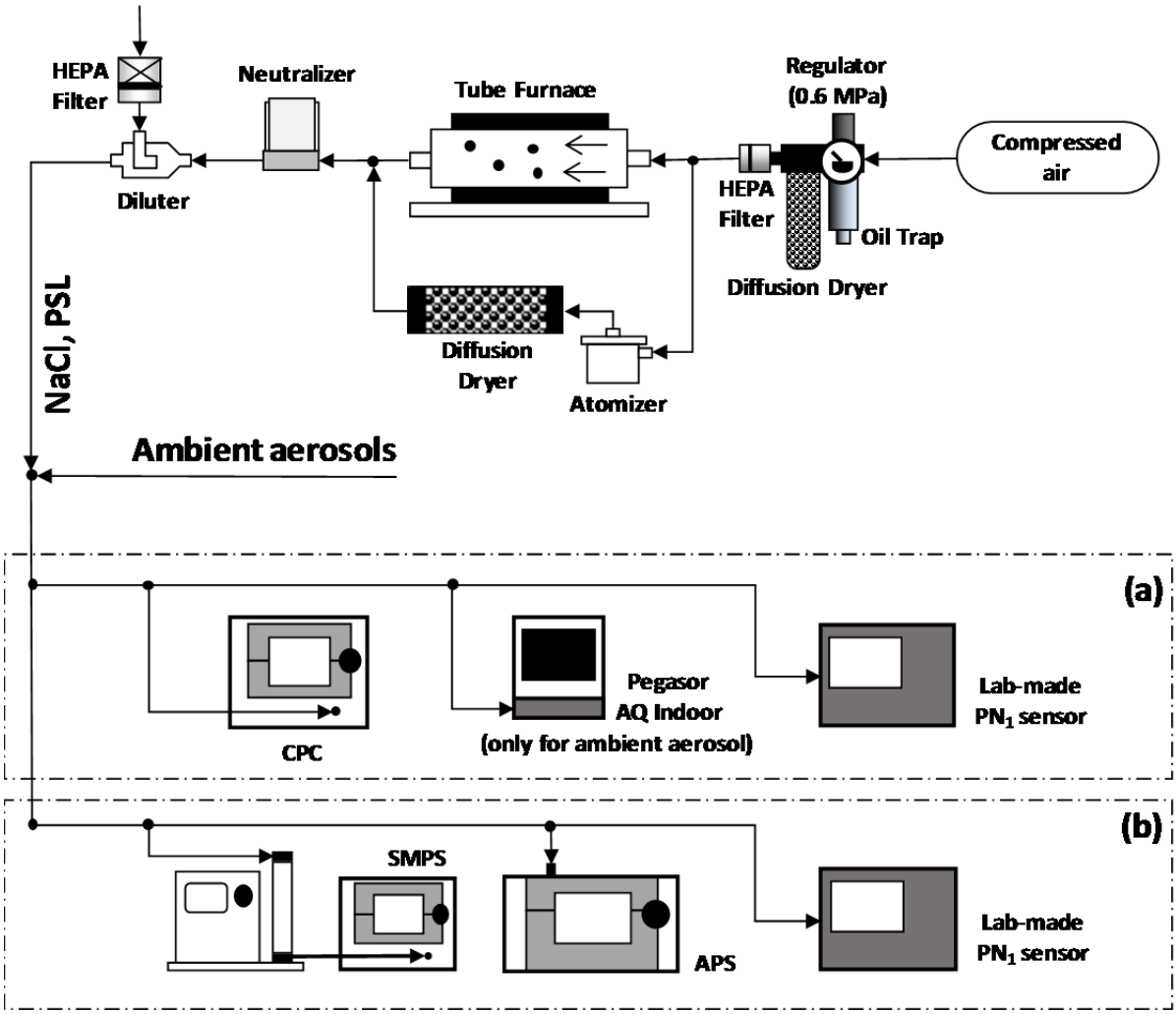

Fig. 3. Schematic diagrams for (a) Number concentration measurement and (b) Geometric mean diameter measurement.

geometric standard deviation, σ_g, is known. After inserting Eqs. (13) and (14) into Eq. (12), we obtain

$$N_{total} = \frac{I_{total}}{e \cdot Q \cdot \alpha \cdot {d_{pg}}^{\beta} \cdot \exp(\frac{\beta^2}{2} \ln^2 \sigma_g)} . \quad (15)$$

For two different voltages applied to the charger, two different currents ($I_{total,1}$ and $I_{total,2}$) are measured, respectively, and the following equation is obtained:

$$\frac{I_{total,2}}{I_{total,1}} = \frac{\alpha_2}{\alpha_1} \times {d_{pg}}^{\beta_2 - \beta_1} \times \exp\left[\frac{(\beta_2 - \beta_1)^2}{2} \ln^2 \sigma_g\right] \quad (16)$$

After the geometric mean diameter is calculated with Eq. (16), the total number concentration can be calculated with Eq. (15).

In addition to lab-test, field test was carried out with indoor aerosols in different places. The temperature and relative humidity were 28–31.5°C and 40–60%, respectively. The aerosol sampling point was about 1 m height from the ground in each place. The number concentration and geometric mean diameter of indoor aerosols were measured by PN_1 sensor and compared with SMPS data. The number concentration was also compared with the results of CPC and Pegasor AQ Indoor (Pegasor, Finland) measurements.

RESULTS AND DISCUSSION

Evaluation of Virtual Impactor

For 4.0 L min^{-1} of inlet flow rate, 3.2 L min^{-1} of major flow rate, and 0.8 L min^{-1} of minor flow rate, the experimentally determined separation efficiencies of the impactor for various particle sizes are shown in Fig. 4 [see Eq. (3)]. The cutoff diameter was 0.96 μm, which was close to the design value of 1 μm. Fig. 4 also shows separation efficiencies determined by CFD calculation with FLUENT [see Eq. (1)]. In the calculation, particles smaller than roughly 1 μm in diameter tended to follow the major flow, but larger particles moved immediately into the minor flow [see Fig. 5(a)]. The calculated cutoff diameter was 0.95 μm, which also supported the design value of 1 μm.

Fig. 4 shows that the maximum wall losses were less than 47% and 60%, respectively, for the numerical calculation and experiment. These wall losses were less than those of previous works; 70% for Marple *et al.* (1980) and 65% for Ding *et al.* (2000). The wall loss was maximal at the cutoff diameter and decreased when the particle diameter exceeded the cutoff diameter. It has been reported that the main cause

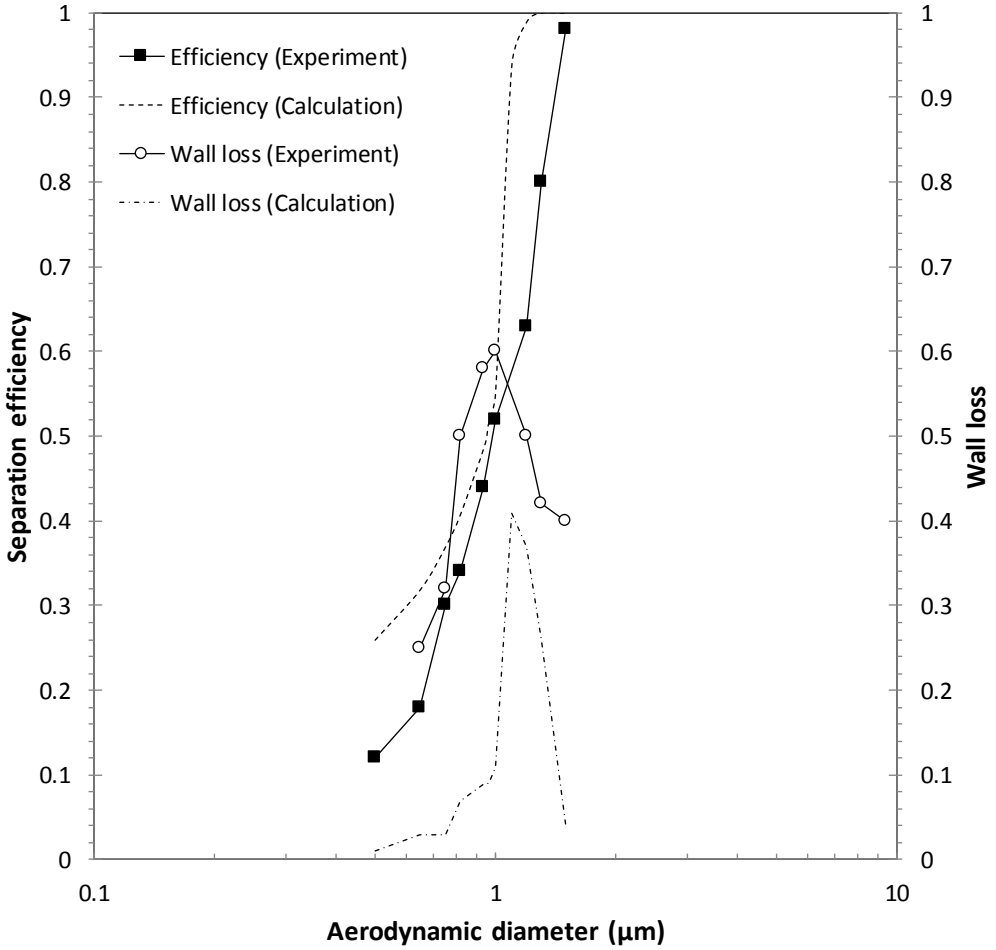

Fig. 4. Separation efficiency and wall loss of impactor (standard deviation of each datum ~4%).

of particle wall loss in a virtual impactor is turbulence in the flow, and the subsequent generation of eddies around the tip of separation channels (Sioutas *et al.*, 1994; Lim and Lee, 2006), which are well presented in Fig. 5(b). One of possible reasons for the difference between our experimental and numerical results is that we assume in the simulation that airflow enters the inlet with a constant, steady-state velocity. However, in a real situation, this assumption might not be valid because air is supplied to the impactor through a tube connection part which has a 90° bend. Therefore, some disturbances, including turbulence, might occur. This argument can also be applied to the outlet parts.

Evaluation of Charger

We measured the corona currents for various applied voltages. As the applied voltage increased beyond the corona starting voltage of about 2.7 kV, the corona current gradually increased, but a spark-over phenomenon occurred at applied voltages greater than about 6 kV. The corona starting voltage predicted by Eq. (7) was 2.9 kV, which

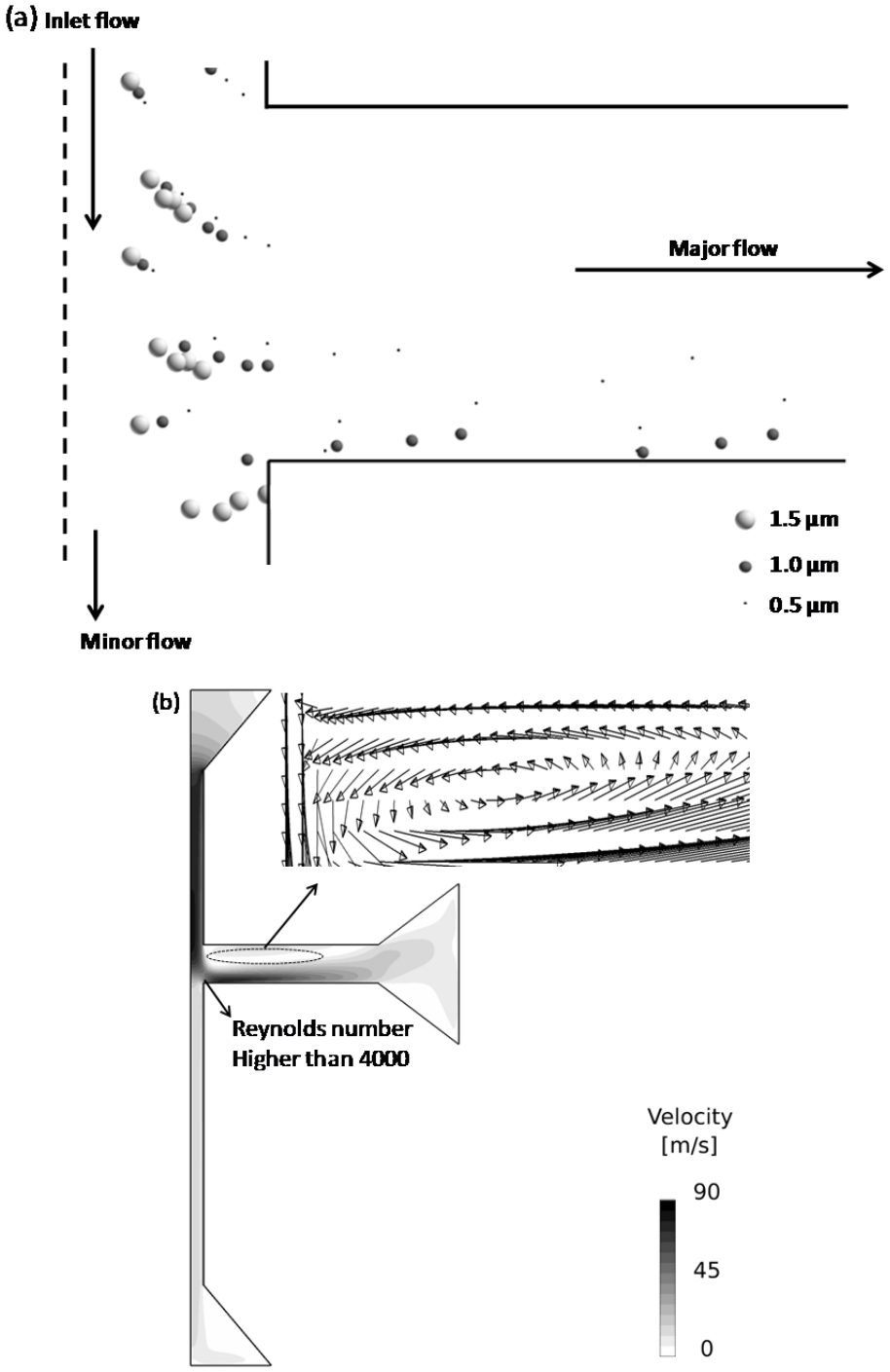

Fig. 5. CFD results for impactor; (a) Particle motion. (b) Air velocity and flow motion.

was close to the measured voltage. The experimental data for the current-voltage characteristics were fit by Eq. (6) with C = 1.1 μA/kV$^{1.5}$ and a =1.5. The ion concentrations N_{ion} estimated by Eq. (5) for 3.0–5.5 kV of applied voltage were 1.58 × 10^{14}–1.13 × 10^{16} # m^{-3}, respectively.

After estimating the ion concentrations, the average particle charge numbers, n_m, were experimentally determined by using Eq. (10) for different particle sizes when the voltages applied to the charger were 3.5, 4.0, and 5.0 kV; the results are shown in Fig. 6(a), which also shows theoretical charge numbers determined by using Eq. (S1) of Supplemental information. Overall, the differences between experimental

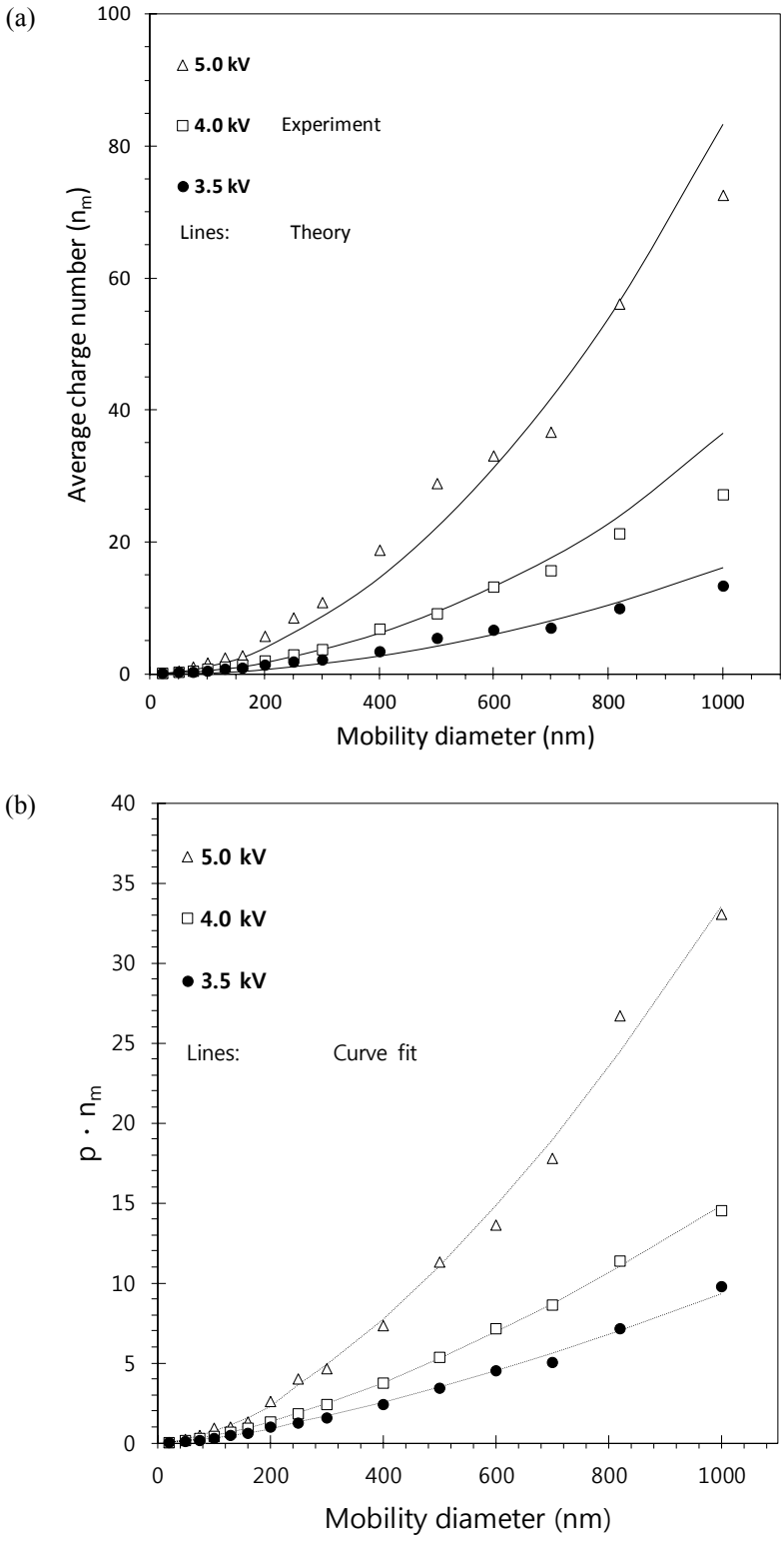

Fig. 6. (a) Average charge number per particle and (b) $p \cdot n_m$ values (standard deviation of each datum ~7%).

and theoretical values were less than 30%. The values for $p \cdot n_m$ are shown in Fig. 6(b) for various particle sizes, where p represents the penetration (= 1 – $WL_{charger}$). The constants α and β determined from the fit by Eq. (13) are summarized in Table 1. The wall losses of the charger were 47% ± 10%, 62% ± 7%, and 72% ± 8% when the voltages applied to the charger were 3.5, 4.0, and 5.0 kV, respectively.

Evaluation of Lab-Made Aerosol Electrometer

The lab-made aerosol electrometer was tested with different particle sizes (20–700 nm) and concentrations (40–30,000 # cm^{-3}) and the results were compared with those obtained with TSI aerosol electrometer (see Fig. 7). The electrical currents carried by these particles varied from 4 to 6000 fA. The difference between the current measured with the lab-made aerosol electrometer and that with the TSI aerosol electrometer was less than 30%. Based on the one-sample t-test, the ratio of currents measured by the lab-made aerosol electrometer to those measured by the commercial aerosol electrometer was not significantly different from the unity ($p > 0.05$).

Evaluation of Number Concentration and Size Distribution with PN_1 Sensor

Fig. 8 shows the comparison results of PN_1 sensor with CPC for different groups of monodisperse NaCl particles between 20 and 700 nm in diameter. Overall, the number concentrations measured with PN_1 sensor and CPC were linearly correlated. The differences between PN_1 sensor and CPC varied from 1.2% to 35%, depending on the particle size (average difference ~14.3%). Asbach *et al.* (2012) measured aerosol number concentration of NaCl (geometric mean diameter of 35.7 nm) by using DiSCmini and NanoTracer and compared the results with CPC data. The differences were less than 25% and 19% with DiSCmini and NanoTracer, respectively. Therefore, our PN_1 sensor predictions were overall reasonable. Mills *et al.* (2013) measured NaCl aerosol number concentrations by using a DiSCmini and a handheld CPC (3007, TSI, MN, USA). They reported that the accuracy of the DiSCmini was reasonable for two groups of particles with monodisperse diameters of 30 and 100 nm. However, for the group of 300 nm NaCl particles, they reported that the number

Table 1. $p \cdot n_m$ values with different applied voltages.

Applied voltage (kV)	$d_p < 200$ nm		$d_p \geq 200$ nm	
	α ($nm^{-\beta}$)	β (-)	α ($nm^{-\beta}$)	β (-)
3.5	4.56×10^{-4}	1.43	5.50×10^{-4}	1.41
4.0	4.89×10^{-4}	1.49	5.03×10^{-4}	1.49
5.0	5.87×10^{-4}	1.56	5.32×10^{-4}	1.60

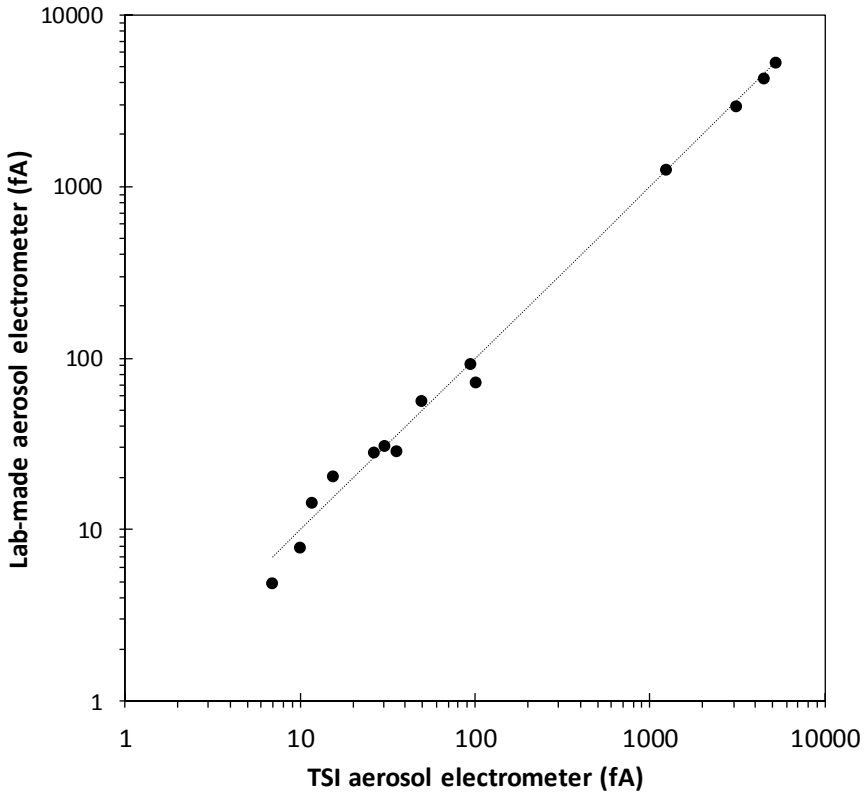

Fig. 7. Comparison of TSI aerosol electrometer with lab-made aerosol electrometer. The number concentration range with CPC is 40 to 30,000 # cm^{-3} (standard deviation of each datum ~7%).

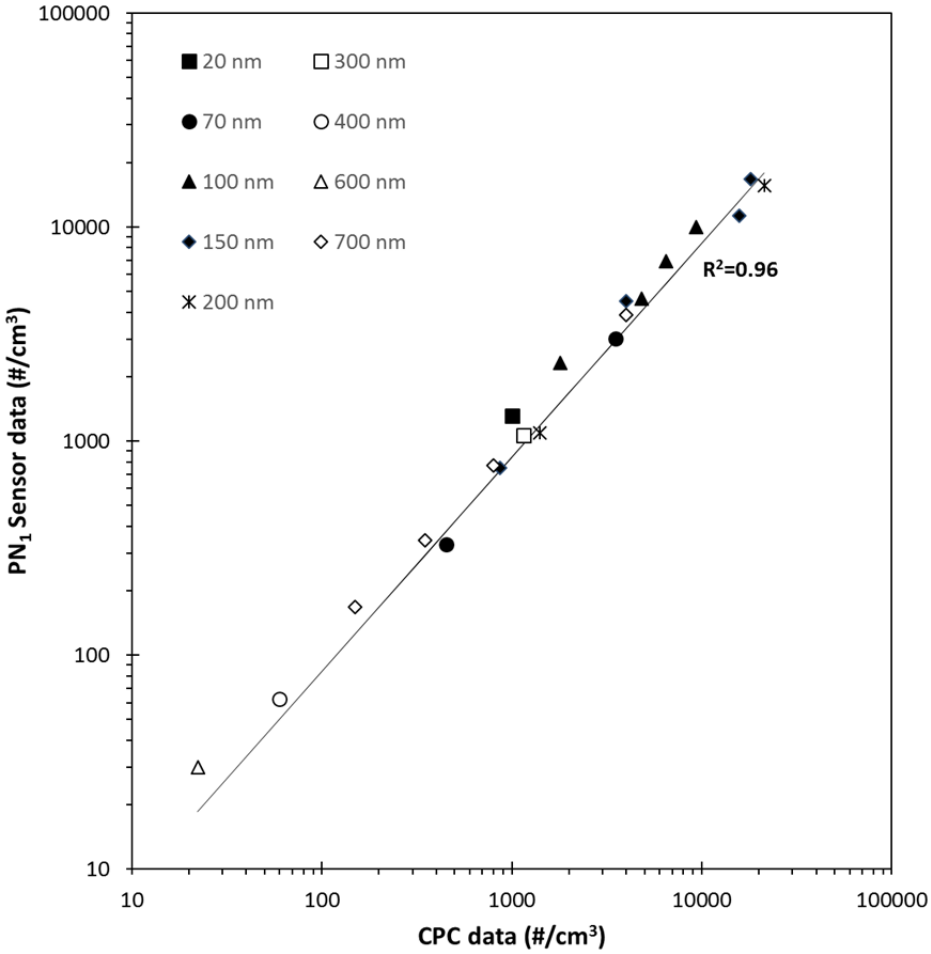

Fig. 8. Comparison between CPC and PN_1 sensor for monodisperse NaCl particles (diameter: 20–700 nm) (standard deviation of each datum ~8%).

concentration was 1.55 to 2.01 times higher than that measured with CPC. On the other hand, the results of Fig. 8 show that our PN_1 sensor predictions were quite good for 300 nm particles and even for particles larger than 300 nm (i.e., 400, 600, and 700 nm).

Fig. 9 compares the results obtained with our PN_1 sensor with those obtained with the SMPS and APS. Our PN_1 sensor data were obtained by varying the combination of two corona voltages and also by varying test particle size distribution. Fig. 9(a) shows the comparison results with SMPS for NaCl particles having 50.6 nm of geometric mean diameter and 3.60×10^3 # cm^{-3} of total number concentration. The best results were obtained the combination of two corona voltages was that of 3.5 kV and 4.0 kV where the geometric mean diameter and the number concentration were 44.81 nm and 4.07×10^3 # cm^{-3}, respectively, resulting in 11.4% and 13.0% differences with the SMPS data. Fig. 9(b) shows the comparison results for NaCl particles having 350.2 nm of geometric mean diameter and 2.87×10^3 # cm^{-3} of total number concentration. The combination of 3.5 kV and 4.0 kV also led to the best results. For this combination, the geometric mean diameter and the total number concentration were 301.3 nm (13.9% difference) and 2.87×10^3 # cm^{-3} (6.29% difference), respectively. On the other hand, the combination of 4.0 kV and 5.0 kV led to the best results when PSL particles having 868.2 nm of geometric mean diameter and 9.21×10^2 # cm^{-3} of total number concentration were used as test aerosols (See APS data of Fig. 9(c)). Our PN_1 sensor results were such that the geometric mean diameter was 789.4 nm (12.2%) and the number concentration was 1.04×10^3 # cm^{-3} (13.0%). The comparison results are summarized in Table 2.

Fig. 10 shows the comparison results of PN_1 sensor with SMPS for measurement of indoor aerosols in two different places. The SMPS data obtained from the underground parking lot (about 100 parking spaces, Fig. 10(a)) show a unimodal distribution. The differences were 20.6% for geometric mean diameters (25.8 nm for SMPS and 31.2 nm for PN_1 sensor) and 8.5% for number concentrations (9.45×10^4 # cm^{-3} for SMPS and 1.03×10^5 # cm^{-3} for PN_1 sensor). On the other hand, the SMPS data of the graduate students (about 40 people) office shows a bimodal-like size distribution (see Fig. 10(b)), while our PN_1 sensor data are based on the assumption of a unimodal size distribution as in other electrical particle-detection sensors such as NanoTracer, DiSCmini, Pegasor AQ Indoor. Nonetheless, the differences between the PN_1 sensor and the SMPS data were 13.3% for geometric mean diameters (73.3 nm for

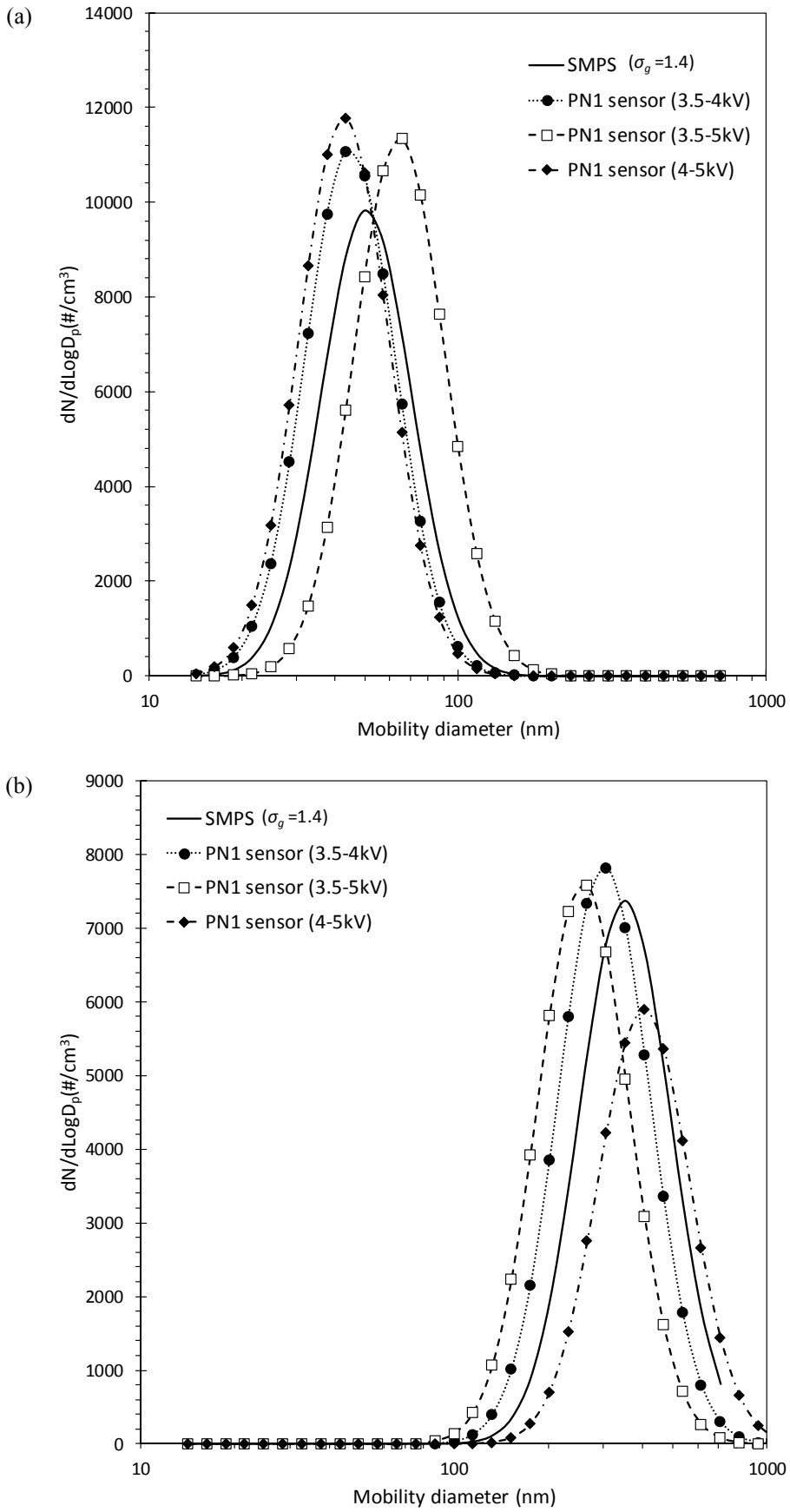

Fig. 9. Particle size distributions obtained by PN_1 sensor, SMPS, and APS; (a) NaCl ($d_{p,mean}$ = 50 nm), (b) NaCl ($d_{p,mean}$ = 350 nm), and (c) PSL ($d_{p,mean}$ = 900 nm).

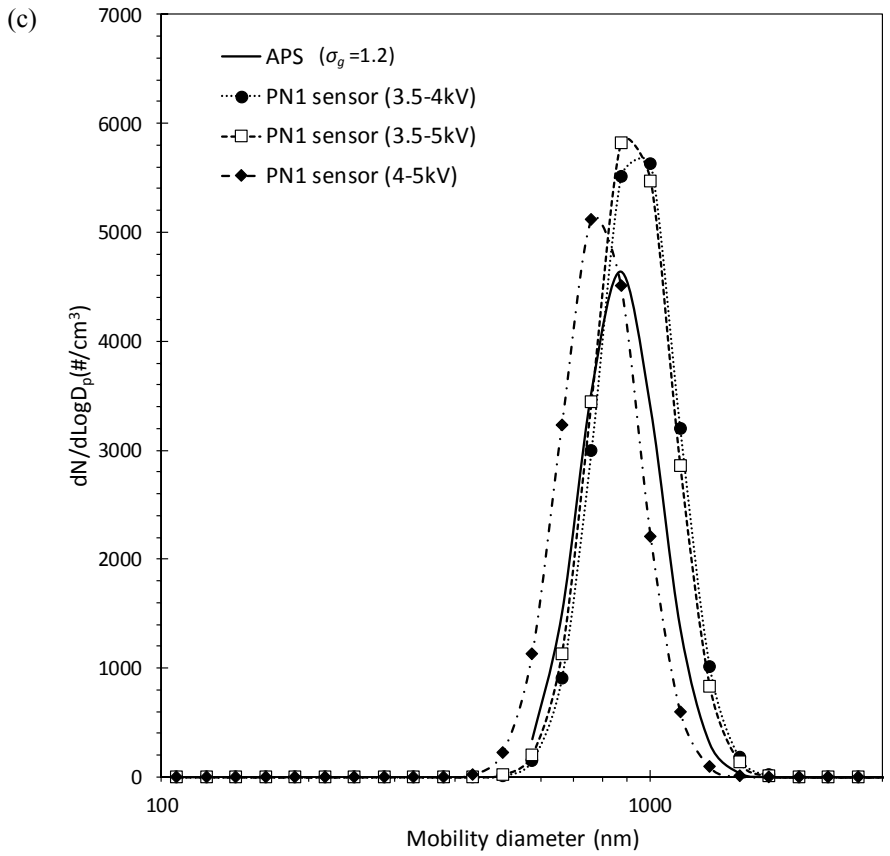

Fig. 9. (*continued*).

Table 2. Size distributions obtained by PN_1 sensor, SMPS, and APS.

	SMPS	APS	PN_1 sensor		
			3.5 and 4.0 kV	3.5 and 5.0 kV	4.0 and 5.0 kV
Geometric Mean diameter (nm)	50.6	-	44.81 (11.4%)	64.69 (27.8%)	42.75 (15.5%)
Number concentration (# cm^{-3})	3.60×10^3	-	4.07×10^3 (13.0%)	4.16×10^3 (15.7%)	4.32×10^3 (20.1%)
Geometric Mean diameter (nm)	350.2	-	301.3 (13.9%)	258.5 (26.4%)	403.8 (15.2%)
Number concentration (# cm^{-3})	2.70×10^3	-	2.87×10^3 (6.29%)	2.79×10^3 (3.33%)	2.16×10^3 (20.0%)
Geometric Mean diameter (nm)	-	868.2	940.5 (4.68%)	922.0 (2.71%)	789.4 (12.2%)
Number concentration (# cm^{-3})	-	9.21×10^2	1.19×10^3 (29.3%)	1.21×10^3 (31.5%)	1.04×10^3 (13.0%)

SMPS and 83.1 nm for PN_1 sensor) and 21.4% for number concentrations (5.26×10^3 # cm^{-3} for SMPS and 6.38×10^3 # cm^{-3} for PN_1 sensor).

It should be noted that our PN_1 sensor results depend on the choice of geometric standard deviation (SD). For example, SD = 1.4 and SD = 1.2 were used for NaCl particles (Figs. 9(a) and 9(b)) and PSL particles (Fig. 9(c)), respectively. When the sensor was used to measure indoor particles suspended in the underground parking lot and office, SD = 1.6 was used (Fig. 10). Therefore, our PN_1 has a limitation since an appropriate value of SD need be determined before the sensor is used in a certain environment.

Fig. 11 shows the comparison results of PN_1 sensor with CPC and also with Pegasor AQ Indoor when the experiments were carried out for indoor aerosols. Pegasor AQ Indoor was selected since it is also based on the electrical detection similar to PN_1 sensor. The regression factors (R^2) were 0.962 and 0.970 with CPC and Pegasor AQ Indoor, respectively. Overall, the results with our PN_1 sensor were in good agreement with those obtained with two commercial instruments, even though there were some discrepancies between CPC and Pegasor AQ Indoor data.

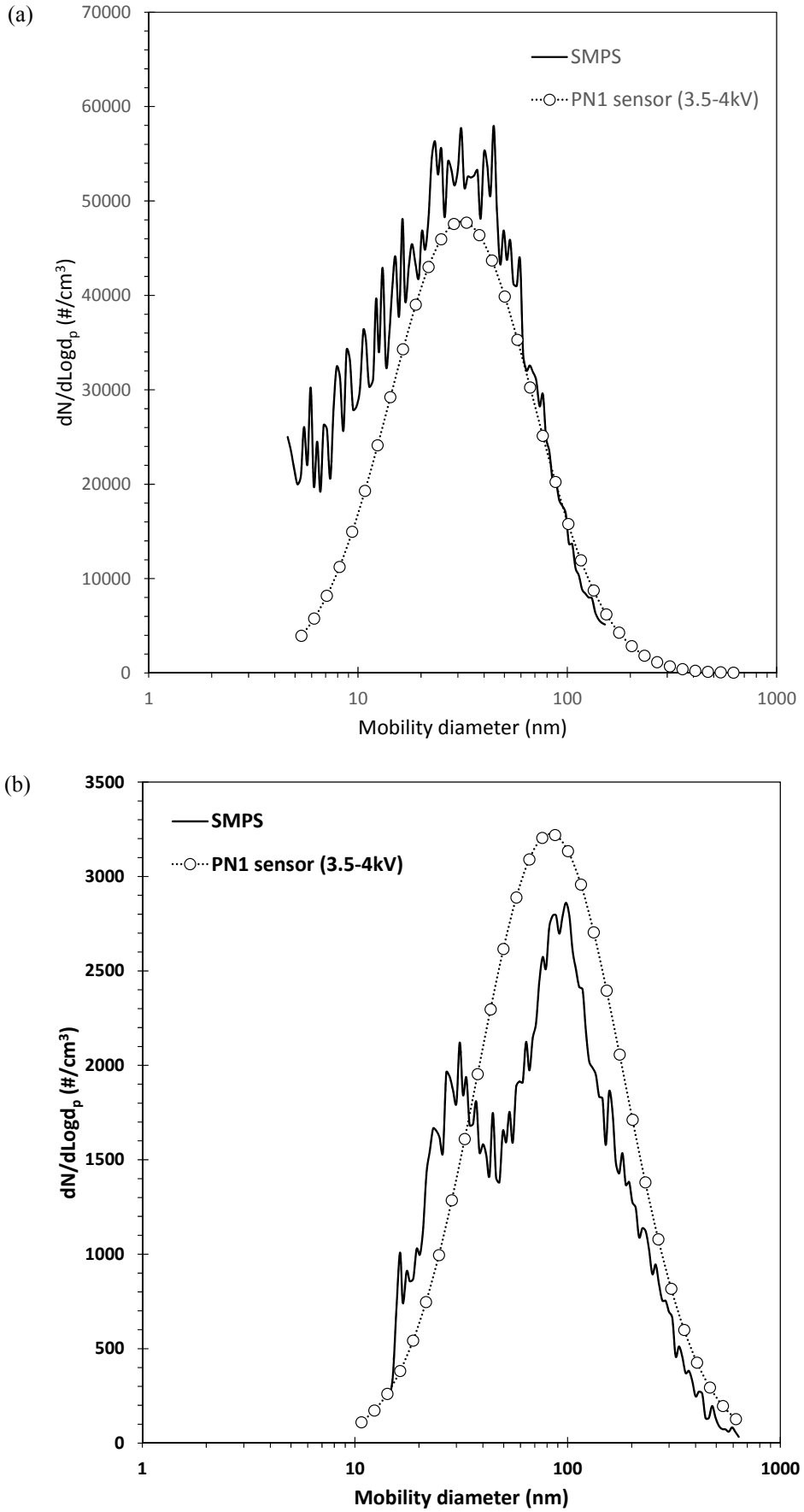

Fig. 10. Particle size distributions obtained by PN_1 sensor and SMPS at (a) underground parking lot and (b) office.

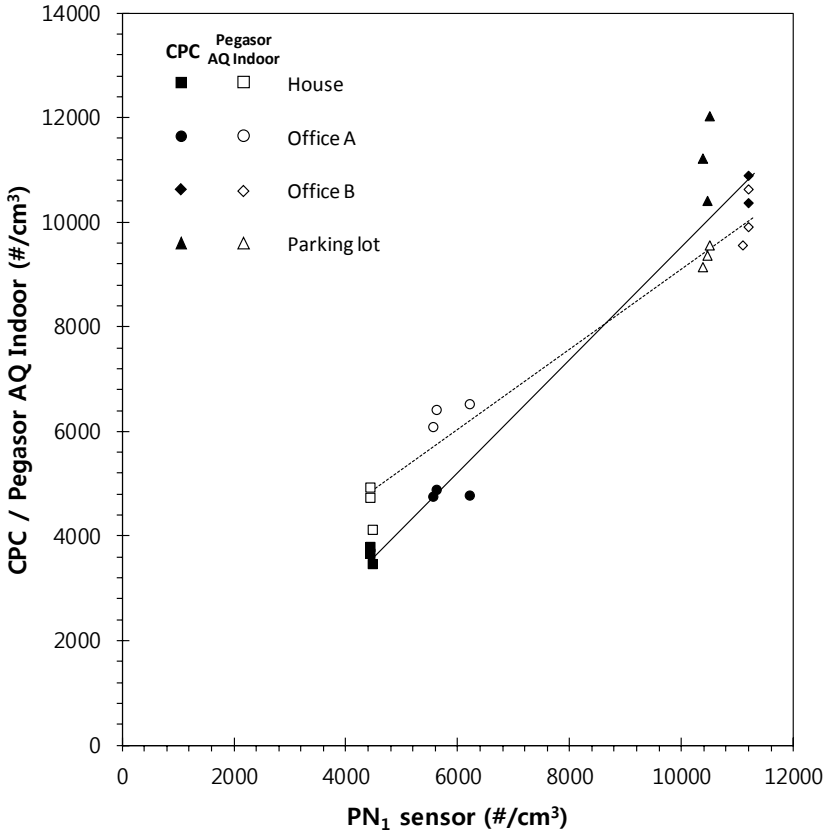

Fig. 11. Comparison between PN_1 sensor with CPC and Pegasor AQ Indoor for ambient aerosols.

It should be noted that our PN_1 sensor can predict more or less inaccurate results if particles in a certain measurement location have bimodal or tri-modal size distributions. Nonetheless, our PN_1 sensor can be used for monitoring indoor particle size distribution in cases of high indoor emission source and indoor activity. According to Lazaridis *et al.* (2017), who measured indoor and outdoor aerosol size distributions in four European cities during 2002 and evaluated the effect of indoor sources on the aerosol size distribution, the percentage of unimodal size distribution increases during indoor emissions, indicating the presence of particles in specific size ranges according to the indoor activity and usually overlapping the multimodal structure of the background aerosol.

CONCLUSIONS

With our miniaturized PN_1 sensor, the total number concentration and geometric mean diameter of test particles were determined using a theoretically developed equation. Two electrical currents corresponding to two different charger voltages, respectively, were applied to the equation. When the PN_1 sensor was compared with a CPC using monodisperse NaCl particles between 20 and 700 nm in diameter, the maximum differences occurred for 20 and 600 nm particle groups and were 31.2% and 35.0%, respectively. When the PN_1 sensor was compared with a SMPS for NaCl particles having two different size distributions (50 and 350 nm of geometric mean diameter), the best results were obtained when the combination of two corona voltages was that of 3.5 kV and 4.0 kV. On the other hand, the combination of 4.0 kV and 5.0 kV led to the best results for the PSL particle size distribution (868.2 nm of geometric mean diameter). The indoor particle size distributions measured by PN_1 sensor were similar with those of SMPS. The total particle concentration obtained by PN_1 sensor for indoor aerosols were in good agreement with those obtained with commercial instruments; CPC and Pegasor AQ Indoor.

ACKNOWLEDGMENT

This research was supported by R&D Center for Green Patrol Technologies through the R&D for Global Top Environmental Technologies funded by Ministry of Environment, Republic of Korea, and also supported by Korean Ministry of Environment (MOE) as “Technologies for Responding to Atmospheric Environment Policies Program”.

SUPPLEMENTARY MATERIAL

Supplementary data associated with this article can be found in the online version at http://www.aaqr.org.

REFERENCES

Abt, E., Suh, H. H., Catalano, P. and Koutrakis, P. (2000).

Relative contribution of outdoor and indoor particle sources to indoor concentrations. *Environ. Sci. Technol.* 34: 3579–3587.

Asbach, C., Kaminski, H., Barany, D.V., Kuhlbusch, T.A.J., Monz, C., Dziurowithz, N., Pelzer, J., Vossen, K., Dietrich, S., Gotz, U., Kiesling, H.J., Schierl, R. and Dahmann, D. (2012). Comparability of portable nanoparticle exposure monitors. *Ann. Occup. Hyg.* 56: 606–621.

Davies, C.N. (1945). Definitive equation for the fluid resistance for sphere. *Proc. Phys. Soc.* 57: 259–270.

Ding, Y. and Koutrakis, P. (2000). Development of a dichotomous slit nozzle virtual impactor. *J. Aerosol Sci.* 31: 1421–1431.

Fierz, M., Burtscher, H., Steigmeier, P. and Kasper, M. (2008). Field measurement of particle size and number concentration with the diffusion size classifier (Disc). *SAE Technical Paper* 2008-01-1179.

Fierz, M., Houle, C., Steigmeier, P. and Burtscher, H. (2011). Design, calibration, and field performance of a miniature diffusion size classifier. *Aerosol Sci. Technol.* 45: 1–10.

Fissan, H., Neumann, S., Trampe, A., Pui, D.Y.H. and Shin, W.G. (2007). Rationale and principle of an instrument measuring lung deposited nanoparticle surface area. *J. Nanopart. Res.* 9: 53–59.

Ji, J.H., Bae, G.N. and Kim, S.S. (2004). Characteristics of aerosol charge neutralizers for highly charged particles. *J. Aerosol Sci.* 35: 1347–1358.

Jung, H. and Kittelson, D.B. (2005) Characterization of aerosol surface instruments in the transition regime. *Aerosol Sci. Technol.* 39: 902–911.

Kaiser, K.L. (2006). *Electrostatic discharge*, CRC press, Florida.

Lazaridis, M., Eleftheriadis, K., Zdimal, V., Schwarz, J., Wagner, Z., Ondracek, J., Drossinos, Y., Glytsos, T., Vratolis, S. and Torseth, K. (2017). Number concentrations and modal structure of indoor/outdoor fine particles in four European cities. *Aerosol Air Qual. Res.* 17: 131–146.

Lee, S.G., Hyun, J., Park, D., Hwang, J. and Kim, Y.J. (2011). Application and performance test of a micro-machined unipolar charger for real-time measurements of exhaust particles from a diesel engine vehicle. *J. Aerosol Sci.* 42: 747–758.

Lim, K.S. and Lee, K.W. (2006). Collection efficiency and particle loss of virtual impactors with different methods of increasing pressure drop. *J. Aerosol Sci.* 37: 1188–1197.

Long, C.M., Suh, H.H. and Koutrakis, P. (2000). Characterization of indoor particle sources using continuous mass and size monitors. *J. Air Waste Manage. Assoc.* 50: 1236–1250.

Loo, B.W. and Cork, C.P. (1988). Development of high efficiency virtual impactors. *Aerosol Sci. Technol.* 9: 167–176.

Marple, V.A. and Chien, C.M. (1980) Virtual Impactors: A theoretical study. *Environ. Sci. Technol.* 14: 976–985.

Marra, J., Voetz, M. and Kiesling, H.J. (2010). Monitor for detecting and assessing exposure to airborne nanoparticles. *J. Nanopart. Res.* 12: 21–37.

Marra, J. (2011). Using the aerasense nanotracer for simultaneously obtaining several ultrafine particle exposure metrics. International conference on safe production and use of nanomaterials. Conference Series 304, 012010.

Meng, X., Zhang, H. and Zhu, J. (2008). A general empirical formula of current-voltage characteristics for point-to-plane geometry corona discharges. *J. Phys. D: Appl. Phys.* 41: 065209.

Mills, J.B., Park, J.H. and Peters, T.M. (2013). Comparison of the DiSCmini aerosol monitor to a handheld condensation particle counter and a scanning mobility particle sizer for submicrometer sodium chloride and metal aerosols. *J. Occup. Environ. Hyg.* 10: 250–258.

Mitsakou, C., Housiadas, C., Eleftheriadis, K., Vratolis, S., Helmis, C. and Asimakopoulos, D. (2007). Lung deposition of fine and ultrafine particles outdoors and indoors during a cooking event and a no activity period. *Indoor Air* 17: 143–152.

Morawska, L., He, C., Hitchins, J., Mengersen, K. and Gilbert, D. (2003). Characteristics of particle number and mass concentrations in residential houses in Brisbane, Australia. *Atmos. Environ.* 37: 4195–4203.

Ott, W.R. and Siegmann, H.C. (2006). Using multiple continuous fine particle monitors to characterize tobacco, incense, candle, cooking, wood burning, and vehicular sources in indoor, outdoor, and in-transit settings. *Atmos. Environ.* 40: 821–843.

Park, D., Kim, Y.H., Lee, S.G., Kim, C., Hwang, J. and Kim, Y.J. (2010). Development and performance test of a micromachined unipolar charger for measurements of submicron aerosol particles having a log-normal size distribution. *J. Aerosol Sci.* 41: 490–500.

Rostedt, A., Marjamaki, M., Yli-ojanpera, J., Keskinen, J., Janka, K., Niemela, V. and Ukkonen, A. (2009). Non-collecting electrical sensor for particle concentration measurement. *Aerosol Air Qual. Res.* 9: 470–477.

Sioutas, C., Koutrakis, P. and Burton, R.M. (1994). Development of a low cut point slit virtual impactor for sampling ambient fine particles. *J. Aerosol Sci.* 25: 1321–1330.

Velasco, E., Siegmann, P. and Siegmann, H.C. (2004). Exploratory study of particle-bound aromatic hydrocarbons in different environments in Mexico City. *Atmos. Environ.* 38: 4957–4968.

Zhang, C., Zhu, R. and Yang, W. (2016). A micro aerosol sensor for the measurement of airborne ultrafine particles. *Sensors* 16: 399–407.

Received for review, August 5, 2017
Revised, December 19, 2017
Accepted, December 27, 2017